Journal of Colloid and Interface Science 607 (2022) 900–911

Contents lists available at ScienceDirect

Journal of Colloid and Interface Science

journal homepage: www.elsevier.com/locate/jcis

Surfactant and dilatational viscosity effects on the deformation of liquid droplets in an electric field

Yu Han [a], Joel Koplik [b], Charles Maldarelli [a]

[a] Levich Institute and Department of Chemical Engineering, City College of the City University of New York, New York, NY 10031, USA
[b] Levich Institute and Department of Physics, City College of the City University of New York, New York, NY 10031, USA

HIGHLIGHTS

- Surfactants affect the deformation of a conducting droplet in an electric field.
- Steady drop deformation is enhanced by surfactants but reduced by surface elasticity.
- Surface dilatational viscosity controls unsteady deformation and delays equilibration.

GRAPHICAL ABSTRACT

(a) A surfactant-covered droplet deformed by uniform electric field; (b) Steady deformation as a function of electric capillary number; (c) Unsteady deformation for various dilatational viscosity values.

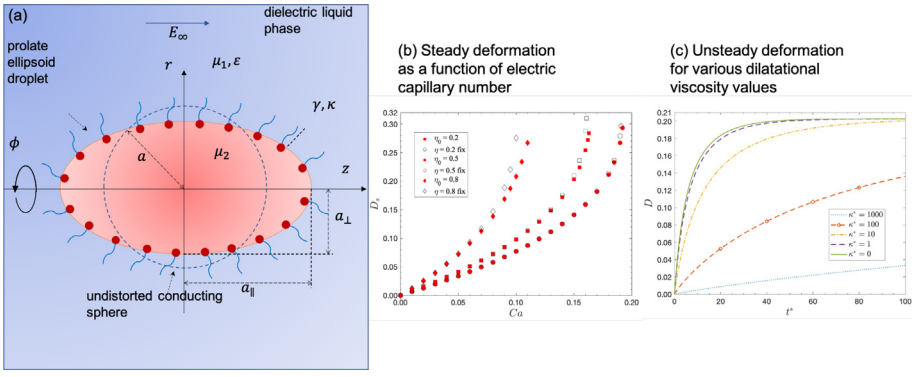

ARTICLE INFO

Article history:
Received 25 November 2020
Revised 11 July 2021
Accepted 19 July 2021
Available online 21 July 2021

Keywords:
Droplet Deformation
Electrocoalescence
Surfactant
Surface Dilatational Viscosity
Asphaltenes
Langmuir isotherm

ABSTRACT

Hypothesis: A conducting droplet suspended in an insulating continuous phase, e.g. an aqueous electrolyte in an oil, is deformed by an applied electric field to nonspherical equilibrium shapes, and can even break-up under strong fields. Many technologies use electro-deformation to manipulate fluid dispersions, with surfactants present on the droplet interfaces forming stabilizing monolayers. While surfactants lower the interface tension which facilitates electro-deformation, the monolayer elasticity resists deformation. High molecular weight surfactants, with large dilatational viscosities, can potentially retard the deformation dynamics.

Numerics: A boundary integral method simulates the dynamic interfacial deformation of a perfectly conducting droplet in a dielectric in a uniform field. The interface contains an insoluble monolayer which is a Newtonian fluid with constant dilatational viscosity obeying a Langmuir state equation. A range of initial surfactant surface concentrations are studied, with elasticity proportional to concentration.

Findings: Equilibrium drop deformations, unaffected by surface viscosity, are strongly resisted by elasticity at high surface concentrations, and field strengths necessary for break-up increase with elasticity. Dilatational viscosity scales with the ratio, κ^*, the surface viscosity (divided by the droplet radius) to the bulk viscosity, and can extend the deformation time. Extended times are described by a time rescaling proportional to κ^*.

https://doi.org/10.1016/j.jcis.2021.07.105
0021-9797/

1. Introduction

When an electric field is applied across a conducting (high dielectric constant) liquid droplet suspended in a continuous, relatively insulating (low dielectric constant) liquid phase, the drop deforms from a spherical shape. A typical example is the electro-deformation of droplets of aqueous electrolytes in nonpolar oils. The deformation arises from the action of the field on the surface charges at the interface, and polarization forces derived from the discontinuity in the dielectric constants at the interface. The interfacial deformation is proportional to the field strength; at low field strengths the drop shape can reach an equilibrium configuration, while at strengths larger than a critical value the droplet can break-up. (For general reviews, see [1–3].) The electric field induced deformation of droplets finds applications in many technological fields. These applications can broadly be divided along two lines: In the first, the electric field is used to induce the fission of the droplets of a suspension, e.g. electroemulsification [4,5] and electrospray ionization for mass spectroscopy [6,7]. In the second, the electric field applied across pairs of droplets deforms each of the droplets, and in addition, due to the fact that the field polarizes each of the droplets in the field direction, drives a dipolar attraction which forces them to approach each other and merge. (electrocoalescence). The key in electrocoalescence applications is to apply field strengths strong enough to induce coalescence without individual drop break-up. Electrocoalescence is an essential unit operation for separating water droplets in a crude oil [8]. Electrocoalescence is also widely used in dropwise microfluidic devices for biological or chemical assays [9,10]. In these applications, on the microfluidic chip, aqueous droplets of reagent reactants are formed separately in an oil phase in which the reactants are not soluble (thus separating the reactants). The droplets are streamed through the flow channels of the chip to a reaction zone where electric fields are applied to merge the droplets and initiate the reaction in a precisely synchronized manner, e.g. [9].

In each of the above applications of the electro-deformation of droplets, surface active agents (surfactants) are present on the interfaces of the droplets. Surfactants on the droplet interfaces form monolayers (or in some cases multilayers) which lower the interfacial tension. Surfactants are either naturally present in the system, or added to facilitate the formation of the dispersion (by the reduction in tension) and to stabilize the dispersion from coalescence. This study focuses on the effect of the surfactant monolayers on the electro-deformation. In principle, surfactants affect the electro-deformation process in several ways. First, they lower the interfacial tension which allows the droplet to be more deformable upon application of the field; as a result, for equilibrium droplets with surfactant monolayers are more deformed than drops without monolayers. Second, surfactant monolayers resist area expansion and contraction; this surface (Gibbs) dilatational elasticity reduces the equilibrium deformation. Finally, surfactant monolayers under areal or shear strain rate can respond as a viscous surface fluid with resultant shear and dilatational stresses. For most low molecular weight surfactants, surface tension lowering and Gibbs elasticity are the important mechanisms. However, for higher molecular weight surfactants or macromolecular surfactants (e.g. proteins) [44], the surface viscous effects become important because the layers are more cohered and multilayers can form. The research to date on electro-deformation of droplets has studied extensively the cases of clean droplet interfaces, and interfaces with surfactants that exert elastic effects. This literature is reviewed in the following section. The influence of viscous effects on the electro-deformation has not been examined, although viscous effects should be important for high molecular weight or macromolecular surfactants, particularly as these can form multilayers which are highly viscous and elastic. The inclusion of surfactant surface viscous effects on electro-deformation is the subject of this theoretical study, where we are particularly interested in how this viscous effect influences the electro-deformation of aqueous droplets in crude oil as part of the electrocoalescence process for dewatering crudes. Crude oils contain asphaltenes and resins which adsorb onto the interfaces of the droplets forming monolayers which have high elasticities and surface viscosities. In these systems, the dilatational viscosity will be important when the bulk viscosity is relatively small and the surface area to volume ratio of the drop is large. For example, as measured by Rane et al. [30], the surface dilatational viscosity of a asphaltene adsorbed water drop in the oil phase has a typical value of around 0.48 mNs/m. The average size of water droplet in the crude oil is around 10 μm and we assume that the viscosity, μ, of the oil phase is 100 cp. Then, the value of the dimensionless surface dilatational viscosity defined as $\kappa^* = \kappa/\mu a$ is around 480 and should not be considered negligible. Studying the influence of surface viscous effects on the electro-deformation will lead to a better understanding of the electrocoalescence process in crude oils. We focus on a solitary perfectly conducting droplet with a surfactant-adsorbed elastic monolayer in a perfectly dielectric liquid medium.

We use the boundary integral method to simulate the axisymmetric deformation of an insoluble surfactant-laden droplet in a uniform electric field. Instead of specifying the mass transport of surfactants along the interface by a convection-diffusion equation, a material coordinate formalism is used to keep track of surface coverage distribution of surfactant. Thus, the surface coverage is computed as the inverse of the local surface area dilation. The droplet and continuous phase are Newtonian fluids with equal viscosities. The interfacial (phase) tension is taken to be isotropic and governed by the Langmuir equation of state which prescribes the elasticity. Furthermore, the surfactant-laden interface is assumed to be a Newtonian surface interface, following Scriven [29]. Only the dilatational surface viscous effect is included with the surface dilatational viscosity, κ, assumed to be a constant. Surface shear viscosity effects can become important, particularly at high surfactant surface concentrations, and this is discussed with the results. The charge relaxation and the charge convection on the interface are not considered.

An outline of this paper is as follows. In Section 2 we briefly summarize past studies of the electo-deformation of droplets, emphasizing the studies on the effect of surfactants. In Section 3, we present the formulation of the problem, some details of the numerical method and the validations of our simulations. In Section 4, the main results are discussed in two parts. First, we discuss the effect of surfactant-adsorbed elastic layer, with a vanishing surface viscosity, on drop deformation. Second, the effect of surface dilatational viscosity on the temporal dynamics of drop deformation is considered. In Section 5, a summary of our work and potential future work is given.

2. Literature review

A great amount of research has been dedicated to an uncharged droplet with clean interface in a steady uniform electric field. Allan and Mason [11] reported experimental observations of prolate spheroidal deformation (major axis parallel to the applied electric field) for conducting droplets and oblate deformation (major axis perpendicular to the applied electric field) for some dielectric drops. For a conducting drop in an insulating liquid, Garton and Krasucki [12] measured the aspect ratio of the critical shape to

be 1.85 before the drop became unstable with increasing electric field.

Taylor [13], introduced a small-deformation theory about a spherical droplet, predicted, and later demonstrated in experiments that the flow circulation pattern inside the droplet depend on the ratios of permittivity and conductivity between the two liquids. The droplet is polarized by electric field along the symmetric axis pointing from one pole to the other. A conducting droplet in an insulating liquid phase is only stretched by the electric field along the symmetric axis through the normal electric stress jump across the interface with vanishing tangential electric stress. If both the continuous phase and droplet are leaky dielectric materials, tangential electric stress jump across the interface, which is only balanced by hydrodynamic viscous stress, will introduce an electrohydodynamic flow with flow direction either from pole to equator or the opposite depending on permittivity and conductivity of the two phases. If the flow is from pole to equator, it could serve as a straining flow stretch the droplet in the direction normal to the symmetric axis resulting an steady oblate ellipsoidal shape [14]. However, when the polarized droplet stretching effect is dominant over the electrohydrodynmic flow effect, the droplet deforms into a steady prolate shape with steady surface flow direction from pole to equator. A 'discriminating function' of the ratios was derived, the sign of which determines whether the drop deformation is prolate or oblate. The steady state deformation as a first-order function of the electric capillary number is also obtained by Taylor [13], and Ajayi [15] extended the function to a more accurate second-order form.

The first numerical calculations based boundary integral method (BIM) to resolve both the electrostatic and the hydrodynamic problems in the Stokes' flow limit is undertook by Sherwood [16]. His work made it feasible to numerically simulate the time-dependent process of droplet deformation and breakup in an electric field. Dubash and Mestel [17] used the BIM to investigate the behavior of a relatively inviscid conducting droplet, corresponding to water in a bitumen or crude oil emulsion, in a uniform electric field. Lac and Homsy [14] used the BIM to explore the dependence of a leaky dielectric droplet and its surrounding liquid on the ratios of their permittivity and conductivity. A wide range of the parameters were investigated and a comprehensive overview of the previous analytical and numerical studies on the more general leaky dielectric droplet is included in their article. For a leaky dielectric droplet, most studies assumed that the charge relaxation (or accumulation) on the interface occurred instantly relative to drop deformation and the charge convection with the surface flow was neglected. More recently Lanauze et al. found, through theoretical analysis [18], BIM calculation [19], and experimental observation [19], that a finite charge relaxation time can induce non-monotonic transient deformation for a droplet attaining oblate steady deformation, while having no influence on the steady state. As shown by Lanauze et al., the slow charge relaxation at the initial stage makes the droplet and the suspending phase behave like a perfectly dielectric system which will always deform toward a prolate configuration. Hence, a droplet would initially distort into a prolate spheroid and later on inversely deform into the steady oblate configuration. Furthermore, they found that charge convection can suppress this steady oblate deformation [19].

When the electric field surpasses the critical strength, the breakup behaviors of conducting droplet in an insulating oil also draw great research interests. Dubash and Mestel [17,20] used the BIM to explore the influence of electric capillary number and viscosity ratio between the droplet and surrounding fluid on the breakup modes. They concluded three different modes right before the onset of breaking up. For relatively inviscid drop and applied electric field near the critical strength, lobes formed at poles of the drop before pinching off. For a more viscous drop, pointed ends forms at the poles before the onset of jetting. And lastly, for intermediate viscosity ratio or high electric capillary number, jets form at rounded (non-pointed) ends of the drop poles. The predicted breakup modes and associated phase diagram were examined and qualitatively confirmed through experiments by Karyappa et al. [21]. They observed the whole breakup process of a droplet, in which the three pre-breakup modes are followed with distinct non-axisymmetric disintegration patterns.

For a droplet with surfactant adsorbed on the interface, the convection of surfactants due to electric field induced flow and the dilution of surfactant due to surface area dilation leads to a surfactant surface coverage variation and an interfacial tension gradient along the drop interface. Aside from affecting the flow, the resulting Marangoni stress also acts to reduce the interfacial tension gradient and can affect the droplet behavior in an electric field. In most of the reported analytical or numerical research, the surfactant is assumed to be insoluble to both bulk phases and its transport on the interface is governed by a form of the convection-diffusion equation. Vizika and Saville [22], following Taylor's small deformation theory, derived a 'discriminating function' showing that the presence of an interfacial gradient tension does not alter the type of droplet deformation in a weak electric field. They assumed that at steady state the convection of the surfactant along the interface is only balanced by surface diffusion. Under the same assumption, Ha and Young [23] extended the analytical work using domain perturbation methods to predict the critical electrical Weber number above which no stable droplet shape can be sustained. Their later experimental work [24] revealed that the surfactant concentration on the interface can affect the breakup mode of the droplet in a steady electric field. Teigen and Munkejord [25] developed a level-set method to numerically simulate the deformation of a surfactant-laden leaky dielectric droplet, in which the rate of change of the surfactant surface concentration is computed from a convection-diffusion equation at each time step. Nganguia et al. [26,27] assumed that, even at large deformation, the surfactant-laden droplet remains a spheroidal shape in a steady electric field. Thus, based on a spheroidal coordinate system, the analytical solution for the flow inside or outside of the droplet is obtained, when the drop shape and the interfacial tension distribution along the interface are given. They simulated the deformation of a leaky dielectric or conducting droplet for various surfactant surface Peclet number ranging from weak diffusivity [26] to diffusivity-dominant transport [27]. In contrast with most of analytical or numerical studies requiring the flow to be axisymmetric, Sorgentone et al. [28] developed a 3D boundary integral method to simulate surfactant-laden droplets in a steady electric field.

3. Problem Formulation

We consider an isolated conducting droplet suspending in a perfectly insulating liquid with uniform external electric field applied. The droplet interface is covered with an insoluble surfactant monolayer. The spherical droplet with radius a is initially at rest. Sup- or Subscripts 1 and 2 will denote the suspending liquid phase and the droplet phase respectively. A schematic of the droplet deformed by the electric field is shown in Fig. 1.

3.1. Electric field and Maxwell Stress

Assume that there is no free charge in the bulk of the droplet phase and the suspending phase. The governing equation for the electric potential, Φ, in the droplet and suspending phases is the Laplace's equation,

$$\nabla^2\Phi = 0. \tag{1}$$

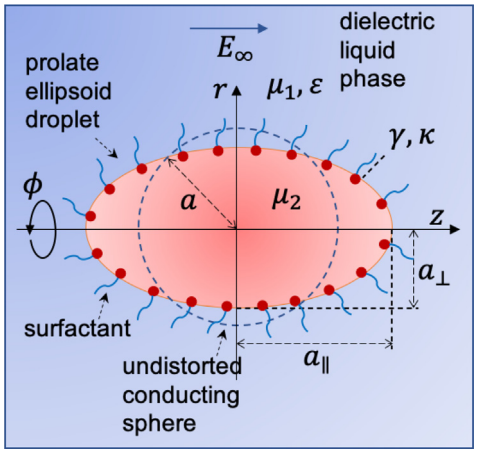

Fig. 1. A schematic of the droplet deformed by the uniform electric field applied horizontally.

The electric field is the space gradient of the potential, $\boldsymbol{E} = -\nabla\Phi$.

The surfactants at the interface introduce a surface layer of dipole moment. In the electrostatic problem, the surface dipole moment is accounted for by a boundary condition, Eq. (2), that there is a electric potential jump across the interface [31].

$$\Delta\Phi = \Phi^{(1)} - \Phi^{(2)} = D_m/(2\varepsilon_0\varepsilon_1) + D_m/(2\varepsilon_0\varepsilon_2) \tag{2}$$

where $1/\varepsilon_2$ goes to 0 as the droplet is conducting and D_m is the surface density of dipole moment which consists of permanent and induced dipole moment.

$$D_m = p\Gamma + \alpha E_s\Gamma \tag{3}$$

where p is the permanent dipole moment of a surfactant molecule, α is the polarizablity, E_s is the electric field strength at the interface and Γ is the surface concentration of surfactant. There are two dimensionless groups,

$$\frac{p\Gamma}{\varepsilon_1\varepsilon_0 E_s a}, \frac{\alpha\Gamma}{\varepsilon_1\varepsilon_0 a}$$

each measuring the ratio of magnitude of surface permanent dipoles or induced dipoles to electrical potential change near the interface respectively. The average permanent dipole moment of asphaltenes measured by Goual and Firoozabadi [32] is ranging from 3.3 to 7.7D which depends on the reservoir sources of the crude oil and whether to precipitate the asphaltenes by n-heptane or n-pentane. To our best knowledge, accurate experimental measurements of average polarizability of asphaltenes has not been reported in the literature. Since the average number of aromatic ring in asphaltene molecules [33] is 7, the average polarizability of coronene [34], $\alpha_{co} = 42.5$ Å, is used to approximate that of average asphaltenes. Substitute the average droplet size $a = 10\mu m$, a typical applied electric field strength $E_\infty = 5kV/mm$, dielectric constant of oil $\varepsilon_1 = 2$, permanent dipole moment $p = 5D$, approximated polarizability $\alpha = 4\pi\epsilon_0\alpha_{co}$ and maximum surface coverage of asphaltenes $\Gamma_\infty = 3.2 molecule/nm^2$ to evaluate both dimensionless groups: $\frac{p\Gamma_\infty}{\varepsilon_1\varepsilon_0 E_\infty a} = 0.060 \ll 1$ and $\frac{\alpha\Gamma_\infty}{\varepsilon_1\varepsilon_0 a} = 0.000086 \ll 1$. Since both of the dimensionless groups are much smaller than 1, we can assume that the surface dipole moment introduced by the asphaltene monolayer has no significant effect on the local electric field strength that we are solving for. Thus, the electric potential is assumed to be continuous across the interface.

Because the droplet is perfectly conducting, the electric field vanishes inside the droplet. In the remainder of the article, we will only look at the the electric field of the insulating suspending phase and drop its subscript for convenience. The center of the initially spherical droplet is set as the origin of the cylindrical coordinate. $R(\boldsymbol{x})$ is the distance between the origin and a point with position $\boldsymbol{x} = \boldsymbol{x}(z, r, \phi)$. The electric field is axisymmetric around the z axis. At far distance away from the conducting droplet, the electric field converges to the applied uniform field $\boldsymbol{E}_\infty$,

$$\Phi(\boldsymbol{x})|_{R(\boldsymbol{x})\to\infty} = -|\boldsymbol{E}_\infty|z = \Phi_\infty(\boldsymbol{x}). \tag{4}$$

Since there is no net charge on the droplet, the surface integral of the field over the droplet surface, S_d, is zero,

$$\int_{S_d} \varepsilon\varepsilon_0 E_n(\boldsymbol{x}) dS(\boldsymbol{x}) = 0 \tag{5}$$

where ε_0 is the vacuum permittivity, ε is the dielectric constant of the insulating suspending phase. $\boldsymbol{n}$ is the unit normal vector of the droplet surface pointing outward and $E_n = \boldsymbol{E}\cdot\boldsymbol{n}$.

The electric (Maxwell) stress, $\boldsymbol{T}^E$, exerted by the field $\boldsymbol{E}$ on the outer side of the surface can be expressed in,

$$\boldsymbol{T}^E = \varepsilon\varepsilon_0\left[\boldsymbol{EE} - \frac{1}{2}(\boldsymbol{E}\cdot\boldsymbol{E})\boldsymbol{I}\right] \tag{6}$$

where $\boldsymbol{I}$ is the unit tensor. The outer electric field at the interface is normal to the surface of the droplet. Thus, there is no tangential electric stress exerted on the interface. The jump in electric stress across the interface can be given as,

$$[\![\boldsymbol{n}\cdot\boldsymbol{T}^E]\!] = \frac{1}{2}\varepsilon\varepsilon_0 E_n^2\boldsymbol{n} \tag{7}$$

where $[\![f]\!] = f_{out} - f_{in}$ denotes the difference of a variable f across the surface.

3.2. Interfacial flow

Both the droplet and the suspending phase are incompressible newtonian fluids. The fluid motion is driven by the electric stress. Thus, a characterisitic velocity can be written as $\varepsilon\varepsilon_0 E_\infty^2 a/\mu_1$, where μ_1 is the dynamic viscosity of the suspending phase. Due to high viscosity of the crude oil, small length scale of the water droplet ($\approx 10\mu m$) and a typical applied electric field of magnitude $10kV/mm$, the Reynold's number $Re = \rho_1\varepsilon\varepsilon_0 E_\infty^2 a^2/\mu_1^2 \ll 1$. Thus, the velocity $\boldsymbol{u}$ and the pressure p of both phases are governed by the Stoke's equation, Eq. (8), where the total hydrodynamic stress is defined as $\boldsymbol{\sigma} = \mu(\nabla\boldsymbol{u} + (\nabla\boldsymbol{u})^\intercal) - p\boldsymbol{I}$, and the continuity equation, Eq. (9).

$$\nabla\cdot\boldsymbol{\sigma} = \boldsymbol{0} \tag{8}$$

$$\nabla\cdot\boldsymbol{u} = 0 \tag{9}$$

With quiescent external field, the velocity vanishes at far distance away from the droplet surface. And the velocity is continuous across the interface. The electric stress is balanced by the hydrodynamic stress and the intrinsic surface stress $\boldsymbol{f}_S$.

$$\boldsymbol{n}\cdot\boldsymbol{T}^E + \boldsymbol{n}\cdot\boldsymbol{\sigma} + \boldsymbol{f}_S = \boldsymbol{0} \tag{10}$$

The surfactant-laden interface is considered as a Newtonian fluid interface described by Scriven [29]. The constitutive equation for the surface stress tensor $T^{\alpha\beta}$ can be written as,

$$T^{\alpha\beta} = \gamma a^{\alpha\beta} + \kappa a^{\alpha\beta}a^{\lambda\mu}S_{\lambda\mu} \tag{11}$$

where γ is the interfacial tension and κ is the surface dilatational viscosity. $a^{\alpha\beta}$ or $a^{\lambda\mu}$ is the contravariant surface metric tensor and $S_{\alpha\beta}$ is the covariant rate of strain tensor, where greek letters denotes the surface coordinates θ^1 and θ^2. For computational purpose, $S_{\alpha\beta}$ can be expressed in terms of the surface covariant derivative of the space velocity, and the detailed derivation is included in Appen-

dix A. We denote the azimuthal angle ϕ as θ^1 and the arc length of the initial meridional contour as θ^2. The expression of $S_{\alpha\beta}$ on the interface embedded in the cylindrical coordinates is included in Appendix B.

The contribution of the surface shear viscosity to the surface stress is neglected. As reported by Harbottle et al. [35], the shear viscous modulus of a asphaltene film at the water-oil interface is around 50 times smaller than the dilatational viscous modulus when the aging time is less than 0.5 hr for various asphaltene concentrations in the continuous oil phase. From our preliminary simulations, when evaluating the surface stress, components of the rate of isotropic strain tensor, which multiplies the dilatational viscosity, and components of the rate of shear strain tensor, which multiplies the shear viscosity, can be comparable. As a result, when surface shear viscosity is much smaller than dilational viscosity, its contribution to the surface stress is negligible. Therefore, when considering applications related to asphaltene films, our assumption is best suited for the monolayer at short aging time.

The surface stress can be written as the combination of the normal and the tangential stress to the surface,

$$\boldsymbol{f}_S = T^{\alpha\beta} b_{\alpha\beta} \boldsymbol{n} + T^{\alpha\beta}_{,\alpha} \boldsymbol{a}_\beta \tag{12}$$

where $b_{\alpha\beta}$ is the covariant curvature tensor and $T^{\alpha\beta}_{,\alpha}$ denotes the surface divergence of $T^{\alpha\beta}$. $\boldsymbol{a}_\beta = \partial \boldsymbol{x}/\partial\theta^\beta$ is the non-unit covariant base vector tangent to the surface.

The interfacial tension γ is given by the Langmuir equation of state as a function of the surface coverage Γ,

$$\gamma(\Gamma) = \gamma_0 + \beta \ln\left(1 - \frac{\Gamma}{\Gamma_\infty}\right) \tag{13}$$

where γ_0 is the clean interfacial tension, Γ_∞ is the maximum surface coverage of the surfactant and $\beta = kT\Gamma_\infty$ is the interfacial elasticity. The surfactant-laden interface is assumed to behave like an elastic membrane during the deformation. Surface diffusion of the surfactant is neglected. And there is no adsorption to the interface from the adjoining phases due to insolubility. Therefore, due to the mass balance, the surface coverage of the surfactant at a material point, $\boldsymbol{x}_s$, on the interface is given by $\Gamma(\boldsymbol{x}_s, t) = \Gamma_0/J_s(\boldsymbol{x}_s, t)$, where $J_s = \sqrt{|A^{\alpha\beta}| \cdot |a_{\alpha\beta}|}$ is the ratio between the deformed and the undeformed local surface area. $|A^{\alpha\beta}|$ and $|a_{\alpha\beta}|$ are the determinants of the undeformed and the deformed metric tensors respectively.

Despite that the surface dilatational viscosity depends on the local surface coverage, κ is assumed to be constant. Because the typical variation in local surface area is less than 10% and the overall effect of the variation in the surface dilatational viscosity on the deformation is expected to be less significant than the gradient of interfacial tension.

3.3. Boundary Integral Equation Representations

Both the electric potential and the velocity field can be expressed in boundary integral equation representations [16] due to the linearity of their governing equations .

Using the free-space Green's function $G(\boldsymbol{x}, \boldsymbol{x}_0) = 1/(4\pi|\boldsymbol{x} - \boldsymbol{x}_0|)$ and the boundary condition Eqs. (4), (1) can be transformed into Eq. (14) [36],

$$\Phi_\infty(\boldsymbol{x}_0) + \int_{S_d} G(\boldsymbol{x}, \boldsymbol{x}_0) E_n(\boldsymbol{x}) dS(\boldsymbol{x}) + \int_{S_d} \Phi(\boldsymbol{x}) \frac{\partial G}{\partial n}(\boldsymbol{x}, \boldsymbol{x}_0) dS(\boldsymbol{x})$$

$$\begin{cases} \Phi(\boldsymbol{x}_0) & \text{for } \boldsymbol{x}_0 \in V_c \quad \text{(a)} \\ \frac{1}{2}\Phi(\boldsymbol{x}_0) & \text{for } \boldsymbol{x}_0 \in S_d \quad \text{(b)} \\ 0 & \text{for } \boldsymbol{x}_0 \in V_d \quad \text{(c)} \end{cases} \tag{14}$$

where $\boldsymbol{x}_0(r_0, z_0, \phi_0)$ is the kernel point, $\Phi_\infty(\boldsymbol{x}_0) = -|\boldsymbol{E}_\infty| z_0$ is the electric potential at $\boldsymbol{x}_0$ in the absence of the droplet, $E_n(\boldsymbol{x}) = -\nabla\Phi(\boldsymbol{x}) \cdot \boldsymbol{n}(\boldsymbol{x})$ is the normal component of the electric field at the interface and $\frac{\partial G}{\partial n}(\boldsymbol{x}, \boldsymbol{x}_0) = \frac{\partial G(\boldsymbol{x}, \boldsymbol{x}_0)}{\partial \boldsymbol{x}} \cdot \boldsymbol{n}(\boldsymbol{x})$. V_c and V_d represent the domains of the suspending and droplet phase respectively.

A standard form of the boundary integral representation is derived as in Eq. (15) [37,38].

$$\boldsymbol{u}_\infty(\boldsymbol{x}_0) - \frac{1}{8\pi\mu_1} \int_{S_d} \boldsymbol{J}(\boldsymbol{x}, \boldsymbol{x}_0) \cdot \boldsymbol{n}(\boldsymbol{x}) \cdot \boldsymbol{\sigma}(\boldsymbol{x}) dS(\boldsymbol{x}) + \frac{1-\lambda}{8\pi} \int_{S_d} \boldsymbol{u}(\boldsymbol{x}) \cdot \boldsymbol{K}(\boldsymbol{x}, \boldsymbol{x}_0) \cdot \boldsymbol{n}(\boldsymbol{x}) dS(\boldsymbol{x})$$

$$\begin{cases} \boldsymbol{u}(\boldsymbol{x}_0) & \text{for } \boldsymbol{x}_0 \in V_c \quad \text{(a)} \\ \frac{\lambda+1}{2}\boldsymbol{u}(\boldsymbol{x}_0) & \text{for } \boldsymbol{x}_0 \in S_d \quad \text{(b)} \\ \lambda \boldsymbol{u}(\boldsymbol{x}_0) & \text{for } \boldsymbol{x}_0 \in V_d \quad \text{(c)} \end{cases} \tag{15}$$

where $\boldsymbol{J}(\boldsymbol{x}, \boldsymbol{x}_0)$ is the Stokeslet, $\boldsymbol{K}(\boldsymbol{x}, \boldsymbol{x}_0)$ is the Stresslet and $\lambda = \frac{\mu_1}{\mu_2}$ is the dynamic visocosity ratio between the suspending phase and the droplet phase. For simplicity of the computation, $\lambda = 1$ such that the double-layer potential (the third term) in Eq. (15) vanishes and the effect of the viscosity difference in the two adjoining phases is not considered. As shown in Section 3.6, the contrast of the viscosity does not affect the steady state deformation. Besides, since we mostly focus on comparing the role of κ and the bulk viscosities played on the dynamic process, it is more explicit to take $\lambda = 1$. $\boldsymbol{u}_\infty$ is the external velocity field which vanishes for the quiescent flow.

Using Eq. (14b) along with the boundary condition at the interface Eq. (5), E_n can be solved numerically after discretizing the droplet surface. Then, the electrical stress at the interface is obtained from Eq. (7). The expression of hydrodynamic stress jump is obtained through the stress balance Eq. (10) at the interface. Substitute it into Eq. (15b) to solve for the velocity field at the interface numerically. The interface evolves according to the kinematic equation,

$$\frac{\partial \boldsymbol{x}_s}{\partial t} = \boldsymbol{u}(\boldsymbol{x}_s). \tag{16}$$

The electric and velocity fields in the two adjoining phases can be obtained from the boundary integral representations.

3.4. Non-dimensionalization

a is the length scale. The stress is scaled by the characateristic clean interfacial stress γ_0/a. The velocity is scaled by γ_0/μ_1 and the time scale is followed as $a\mu_1/\gamma_0$. The whole problem is controlled by four dimensionless groups,

$$Ca = \frac{\varepsilon_0 \varepsilon E_\infty^2 a}{\gamma_0}, \eta_0 = \frac{\Gamma_0}{\Gamma_\infty}, \kappa^* = \frac{\kappa}{a\mu_1}, \beta^* = \frac{kT\Gamma_\infty}{\gamma_0} \tag{17}$$

where the electric capillary number Ca is the ratio of the strength between the electric stress and the clean interfacial stress, η_0 is the initial relative surface coverage, β^* is the relative interfacial elasticity and κ^* is the dimensionless surface dilatational viscosity. Another way to define the capillary number would be using the surfactant-laden interfacial tension with the initial surface coverage, $\bar{Ca} = \varepsilon_0 \varepsilon E_\infty^2 a/\gamma(\eta_0)$.

3.5. Numerical details

Since the electric and velocity fields are axisymmetric, the computational domain can be simplified to the meridional contour $\mathscr{C}$ of the droplet surface. $\mathscr{C}$ is embeded in a (r, z) plane. The curve coordinate $s = \theta^2$ along $\mathscr{C}$ is chosen as the initial arc length of the

meridian of the spherical undeformed droplet such that it is a material coordinate independent of time.

The contour is discretized into N elements bounded by $N+1$ nodes. All nodes are connected by piece-wise cubic splines. At time t, the position of the interface is given by the sum of the cardinal cubic polynomial interpolation functions $Z_j(s)$ or $\overline{Z}_j(s)$ [36],

$$z(s,t) = \sum_{j=1}^{N+1} Z_j(s) z^{(j)}(t) \tag{18A}$$

$$r(s,t) = \sum_{j=1}^{N+1} \overline{Z}_j(s) r^{(j)}(t) \tag{18B}$$

where $Z_j(s)$ has the vanishing first order derivative with respect to s at the poles (the $1st$ and the $(N+1)th$ nodes) and $\overline{Z}_j(s)$ has the vanishing second order derivative at the poles. $\left(z^{(j)}(t), r^{(j)}(t)\right)$, $\left(u_z^{(j)}(t), u_r^{(j)}(t)\right)$ and $E_n^{(j)}(t)$ is the position, velocity and normal electric field strength of the jth node at time t. The electric field and velocity are interpolated in the same manner as the position to guarantee the continuity up to the second order derivative. Note that $\overline{Z}_j(s)$ is used for the interpolation of variables vanishing on the z axis, such as u_r and r, and $Z_j(s)$ is used otherwise.

The surface integrals in Eqs. (14b) and (15b) are first reduced to contour integrals. However, integrating G and $\boldsymbol{J}$ around ϕ result in a logarithmic singularity at the kernel. For elements adjacent to the kernel s_i, the singular integral in the form $\int_{s_i}^{s_{i+1}} f(s)\ln|s-s_i|ds$ or $\int_{s_{i-1}}^{s_i} f(s)\ln|s-s_i|ds$ is first subtracted from the contour integral. The singular part is integrated separately using the special Gaussian quadrature [39] and later added to the remaining regular integral.

At each time step, the interface is interpolated based on the current nodes' positions. The standard boundary element collocation method [36] is used to solve for $E_n^{(j)}, u_r^{(j)}$ and $u_z^{(j)}$. Then,the nodes are advanced by Eq. (16) with the first order explicit Euler method. This process is repeated until it reaches a steady state. Initially, 65 nodes (64 elements) are uniformly distributed along the interface. A more refined node distribution or a higher order node advancing method does not show significant accuracy improvement given the sufficiently small time step. The typical time step we used for the cases of vanishing κ^* is $\Delta t^* = 0.002$. A larger time step is used for κ^* of larger value accordingly. For example, for the case of $\kappa^* = 100$, we pick $\Delta t^* = 0.02$.

3.6. Model Validation

To validate our numerical method, we compare our results with three different cases previously studied in the literature using boundary integral methods. We focus on the steady-state shape of the drop as a function of Ca. The spherical drop deforms into an oval shape, described by the major and minor axes, $a_\parallel$ and $a_\perp$, the aspect ratio $\alpha = a_\parallel/a_\perp$ and the deformation $D = (a_\parallel - a_\perp)/(a_\parallel + a_\perp)$.

In the first case, the surfactant-free interface of a bubble (infinite λ) is considered, instead of the surfactant-laden equal-viscosity situation discussed above. The definition for the electric capillary number is the same as above. The variation of the steady state aspect ratio as a function of Ca, up to the critical value beyond which the droplet will break up, is given by Dubash [17]. In Fig. 2, we see that our results agree perfectly with Taylor's small-deformation theory [13] at small Ca and agree well with Dubash's boundary integral results. Note that the difference in viscosity ratio affects the transient motion of the drop but not the final steady state.

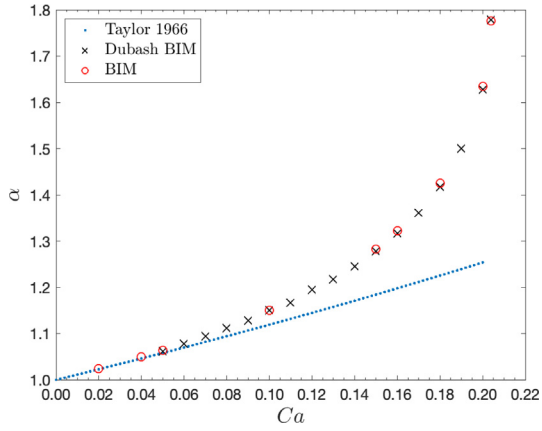

Fig. 2. The steady state aspect ratio α as a function of electric capillary number Ca for a conducting clean droplet in an insulating liquid. The circles and crosses denote our boundary integral method results with $\lambda = 1$ and Dubash's [17] with $\lambda \to \infty$ respectively. The dotted line denotes Taylor's analytical prediction of the first-order small deformation theory [13].

In the second case, there is no applied electric field but instead the axisymmetric deformation of a clean droplet is driven by the elongational flow $\boldsymbol{u}_\infty(\boldsymbol{x}) = (\Omega z, -\Omega r/2, 0)$, where Ω is the local shear rate. The capillary number is defined as $\hat{Ca} = \Omega a \mu_1/\gamma_0$. The steady state deformation D, as a function of the new capillary number $\hat{Ca} = \Omega a \mu_1/\gamma_0$, is given by Stone [40]. In Fig. 3 our results overall agree well with Stone's boundary integral method, here with $\lambda = 1$. The small discrepancy at large $\hat{Ca}$ is attributed to differences in the details of the numerical schemes.

In the third case, a capsule coated with an elastic membrane is deformed by the same elongational flow, $\boldsymbol{u}_\infty(\boldsymbol{x}) = (\Omega z, -\Omega r/2, 0)$. The constitutive equation for the membrane is a neo-Hookean law as given by Lac et al. [43], and the capillary number is defined as $\tilde{Ca} = \Omega a \mu_1/G_s$, where G_s is the surface shear elastic modulus. The exact form of the strain energy function is included in Appendix C.

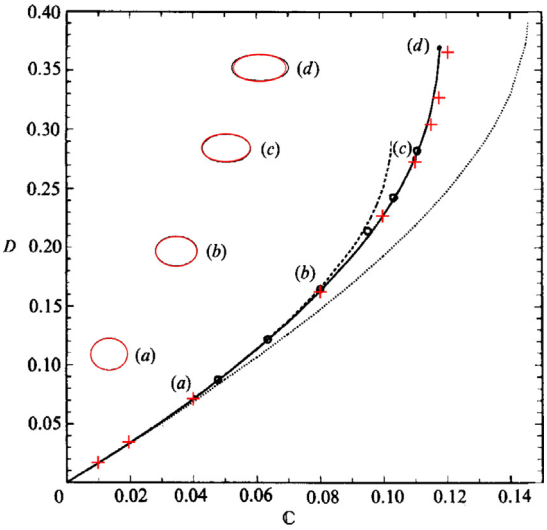

Fig. 3. The steady state deformation D as a function of capillary number $\hat{Ca}(\hat{C})$ for a clean droplet deformed by elongational flow. Our numerical results denoted by crosses are superposed on FIGURE 3 in Stone's work [40] with $\lambda = 1$. The solid line denotes Stone's numerical results by boundary integral method. The dashed lines are Barthès-Biesel and Acrivos'[41] predictions of their small deformation theory, in which the short-dashed curve denotes the first order, $O\left(\hat{Ca}\right)$, and the long-dashed curve denotes the second order, $O\left(\hat{Ca}^2\right)$. Steady shapes (ours denoted by red) are compared for $\hat{Ca} = 0.04, 0.08, 0.11$ and 0.1175.

The steady state deformation as a function of $\tilde{Ca}$ is given by Li and Barthès-Biesel [42]. In Fig. 4 our results show good agreement with the case of initially spherical capsule.

4. Results and Discussion

In this section, we first examine the elastic effect of the adsorbed monolayer, initially ignoring surface dilatational viscosity. We then focus on the specific effects of surface dilatational viscosity.

4.1. Elastic Monolayer

When an electric field is applied to a conducting spherical droplet in an insulating continuous liquid phase, the induced surface flow runs from the poles to the equator of the resulting deformed prolate ellipsoid. We note that the value of the interfacial elasticity number β^* is based on an experimental study of asphaltenes adsorbed at the water-oil interface [30] by Rane et al., where a value of maximum surface coverage for asphaltenes of $\Gamma_\infty = 3.2$ $molecules/nm^2$ at temperature $T = 25\ ^\circ C$ was found. Using a value of $\gamma_0 = 40$ mN/m for the clean interfacial tension, we have $\beta^* = 0.32$. The evolution of droplet shape is shown in Fig. 5a. Initially, the surfactant convecting with the surface flow produces gradients of surface coverage and interfacial tension on the interface, where the regions near to the poles have lower surface coverage and higher interfacial tension. This behavior is exhibited in Fig. 5b where the instantaneous surface coverage is plotted as a function of the axial coordinate z at different times. As indicated in the latter figure, the Marangoni stress exerted on the interface induces surface flow toward the equilibrium state with a uniform surface coverage. Before reaching the steady state, the surface flow due to the electric field induced elongational deformation is countered by the surface flow induced by the Marangoni stress. Thus, the Marangoni effect always suppresses the drop deformation at earlier time when the surface flow is donimated by the electric field induced deformation, as shown at $t^* = 1.6$ in Fig. 5b. While at the later stage, as shown at $t^* = 18$ in Fig. 5b, the surface flow is dominated by the Marangoni effect and the surfactant surface coverage near the poles increases, which means the interfacial tension decreases. Thus, the Marangoni effect could promote the drop deformation at the later stage of the deformation. And finally, at the steady state, the surfactants are distributed uniformly along the interface and there is no surface flow.

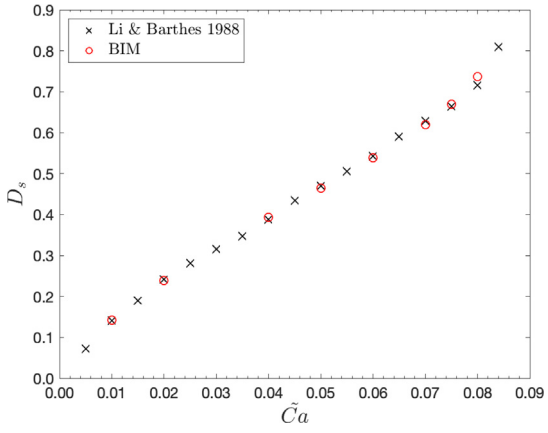

Fig. 4. The steady state deformation D_s as a function of capillary number $\tilde{Ca}$ for an initially spherical elastic capsule deformed by elongational flow. The circles and crosses denote our boundary integral method results and Li's [42] respectively.

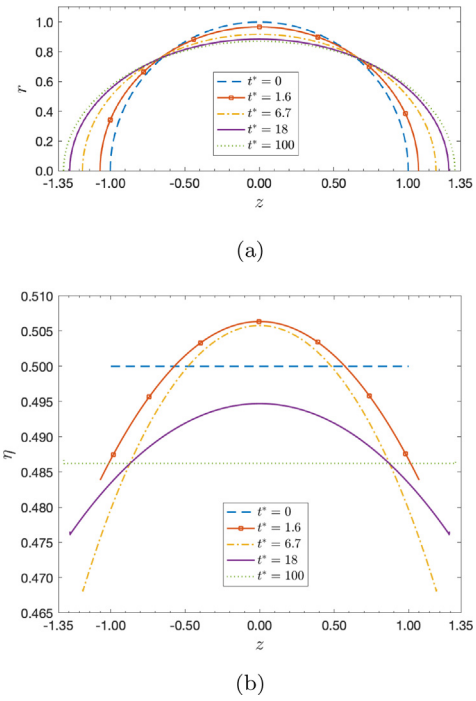

Fig. 5. (a) Snapshot of meridional contour of the droplet at different dimensionless time $t^* = t\gamma_0/a\mu_1$ with $Ca = 0.15, \eta_0 = 0.5$ and $\beta^* = 0.32$. (b) Snapshot of surface coverage η as a function of z along the interface at the corresponding t^* in (a).

The local surface expansion and the sweeping of the surfactants from the poles to the equator of the droplet result in the dilution of the surfactant near the poles. The dilution effect is manifest at earlier times where the surface coverage at the poles has a minimum before the droplet reaches its steady state deformation. The increment of the local interfacial tension due to the dilution suppresses the surface area expansion and the droplet deformation. As a result, the dilution effect is often referred to as an "elastic" effect. We note that the elastic effect is mitigated at the later stage by the Marangoni effect as mentioned above.

To illustrate the significance of the elastic effect combined with the Marangoni effect, we consider a "reference" case where the surface coverage of the surfactant is uniform and fixed during the deformation. In this case the Marangoni stress along the interface vanishes and there is no tangential elastic resistance to the deformation. In Fig. 6, we show the steady state deformation D_s as a function of Ca for three different initial surface coverages η_0, as compared with the corresponding reference cases. We see that deviations from the reference values are larger for larger Ca, meaning that the elastic resistance is more significant at larger steady deformation. At the same D_s, droplets with higher surface coverage η_0 show more elastic resistance to deformation. At the same time, Eq. (13) indicates that higher η_0 yields a smaller interfacial tension, leading to a smaller resistance to the deformation. This behavior is reflected in Fig. 6, where at the same Ca, droplets with higher η_0 have a larger steady state deformation.

When the capillary number Ca exceeds a critical value, the droplet does not reach a steady state shape and continues to deform and eventually breaks up. The critical Ca as a function of the initial surface coverage η_0 is given in Table 1 for $\beta^* = 0.32$, along with the critical values for the fixed-coverage reference cases. We note that the reference Ca_c (fixed η) can also be evaluated based on Ca_c of the clean interface by replacing γ_0 in the definition with the equilibrium surface tension $\gamma_{eq} = \gamma(\eta_0)$. And the evaluated Ca_c (fixed η) underestimates the critical capillary number. On the one hand, droplets with higher η_0 have a smaller critical Ca and will break

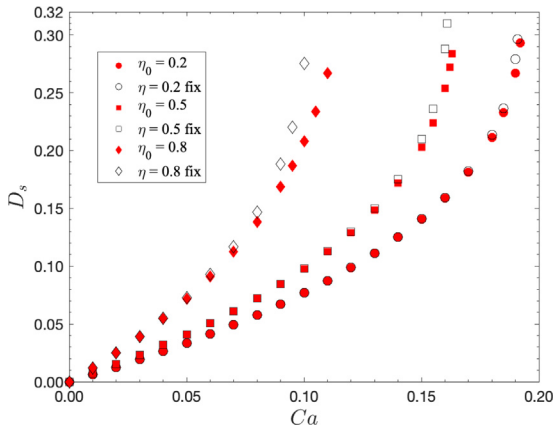

Fig. 6. The steady state deformation D_s as a function of capillary number Ca with $\beta^* = 0.32$ and various initial surface coverage η_0. $\eta_0 = 0.2, 0.5$ and 0.8 are represented by diamonds, boxes and circles respectively. The unfilled markers represent the reference case where the surface coverage η is fixed as η_0 during the deformation.

Table 1
The critical capillary number Ca_c as a function of η_0 with $\beta^* = 0.32$.

η_0	Ca_c	Ca_c (fixed η)
0.2	0.1925	0.1905
0.5	0.1635	0.1595
0.8	0.1120	0.0995

up under a weaker electric field. On the other hand, the deviations from the references show that, again, higher η_0 leads to larger elastic resistance to deformation or break up.

So far, we acknowledge that the significance of the elastic effect is depending on the surface coverage of the surfactant and more noticeable at larger deformation. Next, we examine the dependence of elastic effect on the relative elasticity number β^*. There are three ways of physically varying β^*, varying the temperature, changing the emulsion system, for example, into a ionic liquid in oil emulsion to lower the interfacial tension and having surfactant with different maximum surface coverage at the interface. In Fig. 7, the steady state deformation D_s is showed as a function of β^* for $\eta_0 = 0.5$ along with the 'fixed' references. For all the round markers, the normalized capillary number $\bar{Ca} = \varepsilon_0 \varepsilon E_\infty^2 a/\gamma(\eta_0) = 0.203$

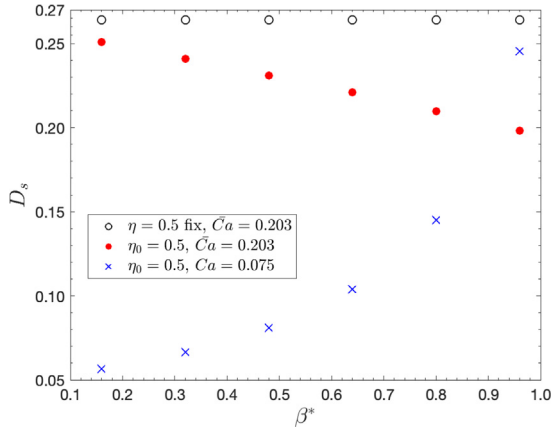

Fig. 7. The steady state deformation D_s as a function of elasticity β^* with $\eta_0 = 0.5$. The circles have the same value of the normalized capillary number $\bar{Ca} = 0.203$. The crosses have the same value of the capillary number Ca.

is the same, such that all the reference cases (unfilled markers) have the same steady state deformation $D_{s,fix}$. From Fig. 7, the deviation of steady state deformation from the reference $\Delta D_s = D_{s,fix} - D_s$ increases linearly with increasing β^*. This observation clearly shows that the interface with higher β^* has a larger elastic effect. However, at fixed Ca (cross markers in Fig. 7), the droplet with higher β^* is more deformed by the electric field. Again, it suggests that the effect of surface tension reduction wins over the elastic effect on the droplet deformation, since a higher β^* also means a greater reduction on the surface tension compared with the clean interface according to Eq. (13).

4.2. The effect of surface dilatational viscosity

As with the bulk viscosity ratio, the value of surface dilatational viscosity κ^* has no effect on the steady state deformation of a droplet, but does contributes to its time evolution. In Fig. 8a this statement becomes clear by plotting the time dependance of the deformation D of the droplet for different values of surface dilatational viscosity. Furthermore, this data can be collapsed by a simple rescaling of time: by choosing an appropriate constant rescaling factor C for each nonzero value of κ^* by hand, Fig. 8b, all curves collapse into that for vanishing κ^*. Note that the scale factors does not have to be modified if we choose a different set of dimensionless groups consisting of Ca, η_0 and β^*. This surprising observation suggests that the value of C only depends on the choice of κ^*.

The scale factor C used to obtain the collapse in Fig. 8a is shown as a function of κ^* in Fig. 8c. As κ^* increases, there is a transition from the nonlinear correlation between C and κ^* to a linear one. Recall that κ^* measures the ratio of magnitude between the surface dilatational viscosity and the bulk phase viscosity. The nonlinear correlation at lower κ^* suggests that the rate of the overall deformation dynamic process is affected by both the bulk phase and the surface diltational viscosity. And the linear correlation at higher κ^* suggests that surface dilatational viscosity dominates over the viscosity of the bulk phase on determining the rate of the dynamic process.

In terms of dilation, as shown in Figure 9 in Harbottle et al.'s [35] and Figure 9 and 10 in Rane et al.'s [30] experimental works, elasticity dominates the asphaltene film's dynamics over viscosity at both early (10 min) and longer (more than 1 hr) aging time for a given frequency around 1.25 Hz. Evolution curves in Fig. 8a can be easily interpreted to include the asphaltene monolayer's elasticity dominant or solid-like behaviors. The elastic effect discussed in this article is in fact a result of the Gibbs elasticity. As we assumed that Langmuir equation is the equation of state, the Gibbs elasticity, E_0, is obtained by its definition [44]:

$$E_0 = -\frac{\partial \gamma}{\partial \ln \Gamma} = \frac{kT\Gamma}{1 - \Gamma/\Gamma_\infty} \tag{19}$$

As Γ approaching the maximum surface coverage Γ_∞, E_0 grows nonlinearly and much faster than the linear dependence. For example, the max relative surface coverage, Γ/Γ_∞, we reported in the paper is 0.8, which corresponds to a E_0 exactly 4 times that of $\Gamma/\Gamma_\infty = 0.5$. For an asphaltene monolayer with $\Gamma/\Gamma_\infty = 0.5$, the dimensional E_0 is evaluated as 12.8 mN/m at $T = 25$ °C. As reported in Fig. 9 in Rane et al.'s article[30], the measured dilational viscous modulus, E'', is around $2.5 mN/m$ at the same interfacial tension, i.e. the same surface coverage, and at a frequency of $f = 1.25$ Hz. Thus, the viscous modulus is less than the elastic modulus, which suggests the formation of a solid-like monolayer for surface coverage $\eta_0 = 0.5$. The dimensionless dilatational viscosity $\kappa^* = \frac{E''}{2\pi f \mu a}$ corresponds to the viscous modulus is around 31 for a water droplet of size $10\mu m$ and a continuous oil phase of viscosity $1000cp$. And the deformation

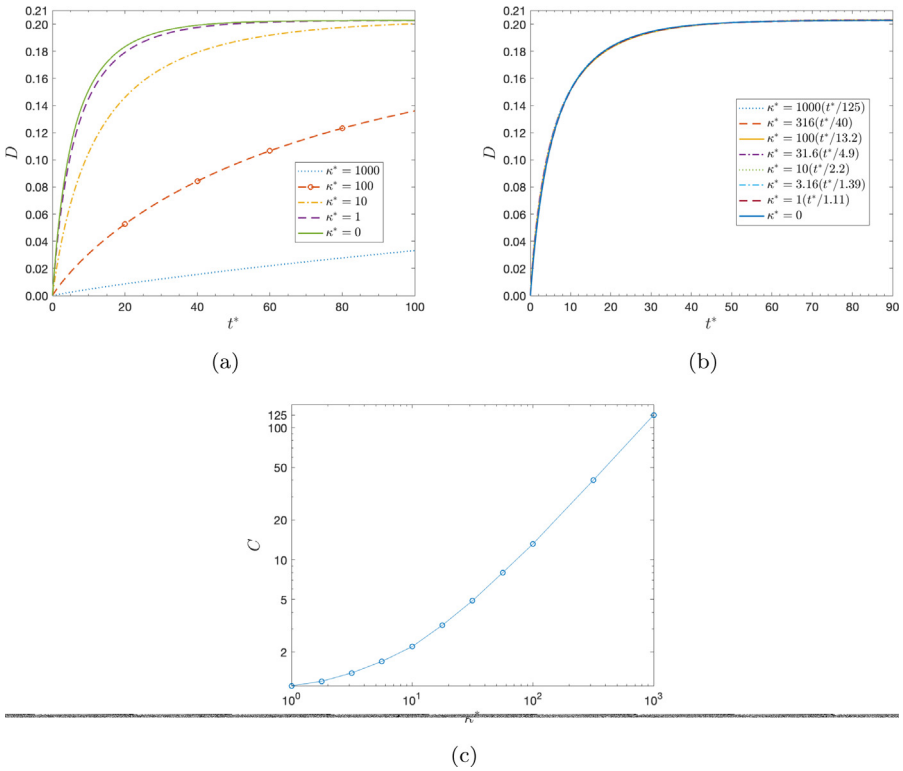

Fig. 8. (a) The droplet deformation as a function of the dimensionless time t^* for different values of κ^* with $Ca = 0.15, \eta_0 = 0.5$ and $\beta^* = 0.32$. (b) The deformation evolution profiles in (a) collapse after rescaling each t^* by a hand-picked constant factor C. (c) C as a function of κ^*.

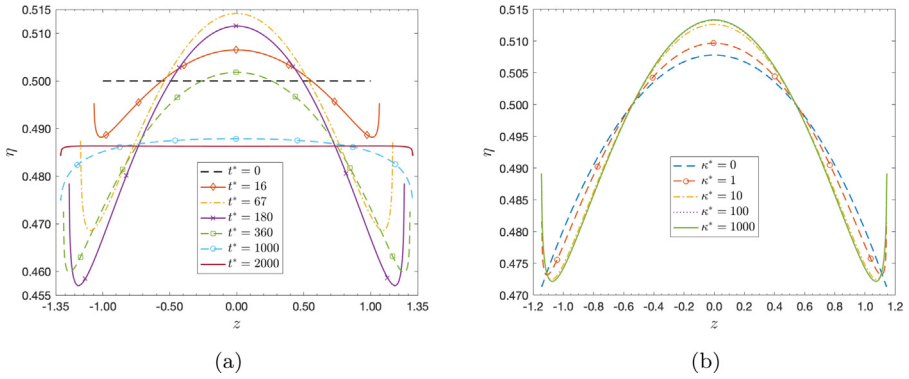

Fig. 9. $Ca = 0.15, \eta_0 = 0.5$ and $\beta^* = 0.32$. (a) Snapshots of surface coverage η as a function of z at various t^*. (b) Snapshots of surface coverage η as a function of z along the interface at the same deformation $D = 0.1$ for different values of κ^*.

evolution curve for $\kappa^* = 31$ should lie in between the curves of $\kappa^* = 10$ and 100 in Fig. 8a. Under the same conditions, $\kappa^* = 1000$ will correspond to a dilational viscous modulus of $75mN/m$ which is much larger than $E_0 = 12.8mN/m$. Thus, the deformation evolution curve for $\kappa^* = 1000$ can be interpreted to represent the dynamics of a surfactant monolayer, other than asphaltene film, in a dilatational viscosity dominant or liquid-like region.

A finite surface dilatational viscosity can also affect the surface coverage distribution of the surfactant along the interface during the deforming process. A sequence of snapshots of the surface coverage distribution for $\kappa^* = 100$ is exhibited in Fig. 9a. At intermediate time, the minimums of η are shifted away from the poles of the ellipsoidal droplet leading to a "W" shaped profile as in contrast with the vanishing κ^* having a parabolic profile. The "W" shaped profile doesn't shift towards an parabolic one until the late stage of the deforming process. And eventually at the steady state, the surface coverage distribution relaxes to a uniform distribution, which takes a longer dimensionless time to reach for nonzero κ^* even after rescaling the time with the factor C. When the droplet starts deforming, the areas near the poles has a larger dilatational rate than the rest of the interface. Thus, the surface viscous effect introduced by nonzero κ^* is more prominent near the poles and restrains the surface flow induced by the electric field leaving the poles, while the flow at the vicinity of the poles is less limited. As a result, the surface coverage minimums are shifted away from the poles but still in their vicinity.

At the same deformation $D = 0.1$, the surface coverage distribution along the interfaces with different κ^* are compared in Fig. 9b. The minimums are lower and further away from the poles for larger κ^*, while the maximum of η at the equator is higher. The obser-

vation that the distribution of η converges for κ^* above 100 suggests that, again, the dynamic deforming process is dominated by surface dilatational viscosity over the bulk viscosity for large κ^*.

5. Conclusion

We have used the boundary integral method to numerically simulate the transient, axisymmetric deformation of a conducting droplet suspended in an insulating liquid under a uniform electric field in the presence of an insoluble surfactant layer on the interface. A Langmuir equation of state describes the tension as a function of the surfactant concentration, and accounts for the layer elasticity. The layer is considered to be a Newtonian surface fluid [29] to take account of surface dilatational viscosity. We investigate the competition between surface tension reduction, surface elasticity, gradients in interfacial tension (Marangoni effect) and surface dilatational viscosity on the drop deformation. The presence of the monolayer always promotes the drop deformation compared with a clean interface under the same electric field strength, due to surface tension reduction. Elastic and Marangoni effects which suppress the overall deformation are more significant at a larger surfactant surface coverage and a larger steady deformation. Our calculations predict the critical field strength beyond which the droplet does not sustain a steady shape. The effect of the dilatational viscosity on the transient dynamics of the electro-deformation of the droplet has not been studied to date. The dilatational viscosity has no influence on the steady state drop shape. (Since the drop is perfectly conducting, there are no electric tangential stresses exerted on the interface, and hence at steady state there is no flow.) We find that as the dilatational surface viscosity increases, the rate of deformation of the droplet in the applied field decreases and in fact the surface dilatational viscosity dominates over bulk viscosity effects at large enough values of the dilatational viscosity. A further effect appears at intermediate times in the spatial distribution of the surfactant; as the dilatational viscosity increases from zero, the minima in the surface coverage shifts away from the droplet poles towards the interior.

Our results extend directly to the applications of electro-deformation of droplets mentioned in the Introduction. In the applications in which the electro-deformation is used to break droplets up (e.g. electroemulsification [5] and electrospraying ionization in mass spectroscopy [45,7]) the timescales for the break-up are critical and our study can directly be used to infer how the timescales are extended by dilatational viscosity effects. In the applications in which the electric field is applied to coalesce droplets (electrocoalescence in the dewatering of crudes [8] and in drop microfluidics for chemical assays [9]), it is important that the imposed fields do not break-up the individual droplets, but only cause them to merge by dipolar forces. The critical electric capillary numbers can be used to estimate the maximum limit of an applied electric field strength in the electrocoalescence process to avoid droplet splitting, especially with the presence of surfactants with large elasticities, such as asphaltenes and resins in crude oil or lipids, proteins or macromolecular surfactants in microfluidic biological assays. More applications of the electro-deformation of droplets which relate to colloid particle-laden droplets and multiphase emulsion droplets are reviewed by Abbasi et al. [3].

Some directions for future work include: (i) The electro-deformation can be affected by the surfactant having a significant surface dipole moment or surface polarizability. In Section 3.1, we noted that two dimensionless groups describe this effect, $\frac{p\Gamma}{\varepsilon_1\varepsilon_0 E_s a}$ (for the permanent dipole moment) and $\frac{\alpha\Gamma}{\varepsilon_1\varepsilon_0 a}$ for the polarizability. While reducing the applied electric field strength does not affect the second group, the first group could be increased such that the permanent dipole moment of surfactant molecules significantly alters the electric stresses on the interface. (ii) Besides surface dilatational elasticity and viscosity of the surfactant monolayer, shear elasticity and viscosity could also be important in determining the single droplet behavior subject to electric fields. For example, for an asphaltene film on the water-oil interface, at a longer aging time (typically more than 1 hr), where additional asphaltene adsorbs to the surface, the shear viscous modulus of the film grows and becomes comparable to the dilatational viscous modulus [35]. More importantly, a measurable shear elastic modulus appears after 1 hr of aging and grows rapidly to be larger than the shear viscous modulus after around 2 hr. This suggests a transition of the asphaltene film microstructure from a liquid-like to a solid-like phase [35]. Future studies critical for applications involving asphaltene or other macromolecule films at the droplet interface will have to include modification to the Newtonian surface model to include a finite shear viscosity and establishing another interfacial constitutive equation for the stress-strain relationship to incorporate shear elasticity. (iii) Finally, our model can be extended to simulate and investigate the electrocoalescence of a droplet pair with the presence of surface active species. In particular, the effect of surface dilatational viscosity is expected to be crucial on the drainage of liquid between the two approaching droplets which is critical to the transient process of electrocoalescence.

Declaration of Competing Interest

The authors declare that they have no known competing financial interests or personal relationships that could have appeared to influence the work reported in this paper.

Acknowledgements

This research was supported by the National Science Foundation under grant No. 1743794, PIRE: Investigation of Multi-Scale, Multi-Phase Phenomena in Complex Fluids for the Energy Industries, and by the Petroleum Research Fund under grant ACS-PRF 57515-ND9.

Appendix A. Surface Rate of Strain Tensor

The surface rate of strain tensor, $S_{\alpha\beta}$, can be expressed intrinsically in terms of the time derivatives of surface metric tensor and the surface covariant derivatives of covariant surface velocity,

$$S_{\alpha\beta} = \frac{1}{2}\dot{a}_{\alpha\beta} + \frac{1}{2}\left(V_{\alpha,\beta} + V_{\beta,\alpha}\right) \tag{A.1}$$

where $\dot{a}_{\alpha\beta} = \frac{\partial a_{\alpha\beta}}{\partial t}$ and $V_\alpha = a_{\alpha\beta}V^\beta = a_{\alpha\beta}\frac{d\theta^\beta}{dt}$. In this section, we show that $S_{\alpha\beta}$ can also be expressed by using surface covariant derivatives of spatial velocity, U^j. This is a reiteration of the Section 10.42 of Aris' book [46]. We then obtain the expression of $S_{\alpha\beta}$ of a moving axisymmetric surface embedded in the cylindrical coordinate. In the following, Greek and Latin subscripts and superscripts represent the surface and the space coordinates, respectively.

The space coordinates of a point on the surface can be written as a function of the surface coordinates and time, $x^i = x^i(\theta^1, \theta^2, t)$. The hybrid tensor that links the surface and the space coordinate system is defined as,

$$t^i_\alpha = \frac{\partial x^i}{\partial \theta^\alpha}. \tag{A.2}$$

The space velocity of a fluid particle in the surface is

$$U^i = \frac{dx^i}{dt} = \frac{\partial x^i}{\partial \theta^\alpha}\frac{d\theta^\alpha}{dt} + \frac{\partial x^i}{\partial t} = t^i_\alpha V^\alpha + \dot{x}^i. \tag{A.3}$$

Based on the identity $a_{\alpha\beta} = g_{ij}t^i_\alpha t^j_\beta$, where g_{ij} is the space metric tensor, the covariant surface velocity can be expressed as

$$V_\alpha = g_{ij}t^i_\alpha\left(U^j - \dot{x}^j\right). \tag{A.4}$$

Based on identities, $g_{ij,\beta} = 0$ and $t^i_{\alpha,\beta} = n^i b_{\alpha\beta}$, the surface covariant derivative of V_α is

$$\begin{aligned} V_{\alpha,\beta} &= g_{ij}\left[t^i_\alpha\left(U^j - \dot{x}^j\right)\right]_{,\beta} \\ &= g_{ij}n^i b_{\alpha\beta}\left(U^j - \dot{x}^j\right) + g_{ij}t^i_\alpha\left(U^j_{,\beta} - \dot{x}^j_{,\beta}\right), \end{aligned} \tag{A.5}$$

where the surface covariant derivative is denoted by subscript $_{,\beta}$ and the space covariant derivative is denoted by subscript $_{,k}$. Regarded as a space vector, t^i_α is tangential to the surface, thus $n_i t^i_\alpha = 0$. Contracting the normal vector n_i into both sides of Eq. (A.3) yields $g_{ij}n^i\left(U^j - \dot{x}^j\right) = 0$. Substitute this identity into Eq. (A.5) we have

$$V_{\alpha,\beta} = g_{ij}t^i_\alpha\left(U^j_{,\beta} - \dot{x}^j_{,\beta}\right) \tag{A.6}$$

The time differentiation of $a_{\alpha\beta}$ is with θ^α held constant. It can be written as

$$\dot{a}_{\alpha\beta} = \frac{\partial}{\partial t}\left(g_{ij}t^i_\alpha t^j_\beta\right) = \frac{\partial g_{ij}}{\partial t}t^i_\alpha t^j_\beta + g_{ij}\left[\frac{\partial t^i_\alpha}{\partial t}t^j_\beta + t^i_\alpha\frac{\partial t^j_\beta}{\partial t}\right]. \tag{A.7}$$

Since a space point, $x^k = x^k(t)$, on the surface is moving with the surface, we have g_{ij} as a function of time, $g_{ij} = g_{ij}(x^k(t))$. Based on the definition of the space covariant derivative, $g_{ij,k} = \frac{\partial g_{ij}}{\partial x^k} - \Gamma^m_{ki}g_{mj} - \Gamma^m_{jk}g_{im}$, where Γ^m_{ki} is the space Christoffel symbol, and the property of the space metric tensor $g_{ij,k} = 0$, we have the identity $\frac{\partial g_{ij}}{\partial x^k} = \Gamma^m_{ki}g_{mj} + \Gamma^m_{jk}g_{im}$. Thus,

$$\frac{\partial g_{ij}}{\partial t} = \frac{\partial g_{ij}}{\partial x^k}\dot{x}^k = \left[\Gamma^m_{ki}g_{mj} + \Gamma^m_{jk}g_{im}\right]\dot{x}^k \tag{A.8}$$

Substituting the identity $\frac{\partial t^i_\alpha}{\partial t} = \frac{\partial \dot{x}^i}{\partial \theta^\alpha}$ and Eq. (A.8) into Eq. (A.7), we have

$$\dot{a}_{\alpha\beta} = g_{ij}\left(\dot{x}^i_{,\alpha}t^j_\beta + t^i_\alpha\dot{x}^j_{,\beta}\right) \tag{A.9}$$

Finally substitute Eqs. (A.6) and (A.9) into Eq. (A.1), we reach the desired form of $S_{\alpha\beta}$,

$$S_{\alpha\beta} = \frac{1}{2}g_{ij}\left(t^i_\alpha U^j_{,\beta} + t^i_\beta U^j_{,\alpha}\right) \tag{A.10}$$

Appendix B. $S_{\alpha\beta}$ on the surface embedded in cylindrical coordinates

We take the cylindrical coordinates as the space coordinates and denote that $x^1 = \phi, x^2 = r$ and $x^3 = z$. The space covariant metric tensor follows as

$$g_{ij} = \begin{pmatrix} r^2 & 0 & 0 \\ 0 & 1 & 0 \\ 0 & 0 & 1 \end{pmatrix}. \tag{B.1}$$

As for the surface coordinates, $\theta^1 = \phi$ and $\theta^2 = s$, where s is the arc-length along the meridional contour of the initial axisymmetric droplet surface. For convenience, the partial derivative of a function f with respect to s is denoted as $f' = \frac{\partial f}{\partial s}$. The surface covariant vector and the normal vector to the surface can be written as

$$\boldsymbol{a}_1 = r\boldsymbol{e}_\phi,\ \boldsymbol{a}_2 = r'\boldsymbol{e}_r + z'\boldsymbol{e}_z, \tag{B.2}$$

$$\boldsymbol{n} = \frac{z'}{\sqrt{z'^2 + r'^2}}\boldsymbol{e}_r - \frac{r'}{\sqrt{z'^2 + r'^2}}\boldsymbol{e}_z, \tag{B.3}$$

where $\boldsymbol{e}_\phi, \boldsymbol{e}_r$ and $\boldsymbol{e}_z$ are unit basis vectors of the cylindrical coordinates. The surface metric tensor is then

$$a_{\alpha\beta} = \begin{pmatrix} r^2 & 0 \\ 0 & z'^2 + r'^2 \end{pmatrix}. \tag{B.4}$$

All the non-zero surface Christoffel symbols $\bar{\Gamma}^\beta_{\alpha\rho}$ are

$$\bar{\Gamma}^1_{12} = \bar{\Gamma}^1_{21} = \frac{r'}{r},\ \bar{\Gamma}^2_{11} = \frac{-rr'}{z'^2 + r'^2},\ \bar{\Gamma}^2_{22} = \frac{r'r'' + z'z''}{z'^2 + r'^2}. \tag{B.5}$$

while the non-zero space Christoffel symbols Γ^i_{jk} are

$$\Gamma^1_{12} = \Gamma^1_{21} = \frac{1}{r},\ \Gamma^2_{11} = -r. \tag{B.6}$$

The non-zero components of the hybrid tensor t^i_α are

$$t^1_1 = 1,\ t^2_2 = r',\ t^3_2 = z'. \tag{B.7}$$

Since the covariant surface derivative of the space velocity is $U^i_{,\alpha} = \frac{\partial U^i}{\partial u^\alpha} + \Gamma^i_{jk}t^j_\alpha U^k$, all non-zero component of $U^i_{,\alpha}$ are

$$U^1_{,1} = \frac{U_r}{r},\ U^2_{,2} = U'_r,\ U^3_{,2} = U'_z, \tag{B.8}$$

where $U_r = U^2$ and $U_z = U^3$ are the component of the space velocity for r and z direction respectively. According to Eq. (A.10), the non-zero components of $S_{\alpha\beta}$ are

$$S_{11} = rU_r,\ S_{22} = r'U'_r + z'U'_z. \tag{B.9}$$

The surface dilatational rate is then

$$\Theta = a^{\alpha\beta}S_{\alpha\beta} = \frac{U_r}{r} + \frac{\left(r'U'_r + z'U'_z\right)}{z'^2 + r'^2} \tag{B.10}$$

Appendix C. Strain Energy Function

We assume that the strain energy function, W, for a capsule with elastic membrane is governed by the neo-Hookean law and we adapt the form of W given by Lac et al. [43] to match with the one used by Li and Barthès-Biesel [42].

$$W(I_1, I_2) = \frac{1}{6}G_s\left(I_1 - 1 + \frac{1}{I_2 + 1}\right), \tag{C.1}$$

where G_s is the surface elastic modulus and the invariants I_1 and I_2 are defined as,

$$I_1 = A^{\alpha\beta}a_{\alpha\beta} - 2,\ I_2 = |A^{\alpha\beta}| \cdot |a_{\alpha\beta}| - 1 = J_s^2 - 1. \tag{C.2}$$

$|A^{\alpha\beta}|$ and $|a_{\alpha\beta}|$ are the determinants of the undeformed contravariant and the deformed covariant surface metric tensors respectively. $J_s = \sqrt{|A^{\alpha\beta}| \cdot |a_{\alpha\beta}|}$ is the ratio between the deformed and the undeformed local surface area. The isotropic surface stress tensor $T^{\alpha\beta}$ for the elastic capsule can be obtained from W as

$$T^{\alpha\beta} = \frac{2}{J_s}\frac{\partial W}{\partial I_1}A^{\alpha\beta} + 2J_s\frac{\partial W}{\partial I_2}a^{\alpha\beta}. \tag{C.3}$$

References

[1] James R. Melcher, Continuum Electromechanics, Cambridge, MA: MIT press, 1981.
[2] P.M. Vlahovska, Electrohydrodynamics of drops and vesicles, Annu. Rev. Fluid Mech. 51 (2019) 305–330.
[3] M.S. Abbasi, R. Song, S. Cho, J. Lee, Electro-hydrodynamics of emulsion droplets: Physical insights to applications, Micromachines 11 (10) (2020) 942.

[4] T. Scott, W. Sisson, Droplet size characteristics and energy input requirements of emulsions formed using high-intensity-pulsed electric fields, Separation Science and technology 23 (12–13) (1988) 1541–1550.
[5] R.B. Karyappa, A.V. Naik, R.M. Thaokar, Electroemulsification in a uniform electric field, Langmuir 32 (1) (2016) 46–54.
[6] S.J. Gaskell, Electrospray: principles and practice, Journal of mass spectrometry 32 (7) (1997) 677–688.
[7] R.L. Grimm, J.L. Beauchamp, Dynamics of field-induced droplet ionization: time-resolved studies of distortion, jetting, and progeny formation from charged and neutral methanol droplets exposed to strong electric fields, J. Phys. Chem. B 109 (16) (2005) 8244–8250.
[8] J.S. Eow, M. Ghadiri, Electrostatic enhancement of coalescence of water droplets in oil: a review of the technology, Chem. Eng. J. 85 (2–3) (2002) 357–368.
[9] K. Ahn, J. Agresti, H. Chong, M. Marquez, D.A. Weitz, Electrocoalescence of drops synchronized by size-dependent flow in microfluidic channels, Appl. Phys. Lett. 88 (26) (2006) 264105.
[10] D.R. Link, E. Grasland-Mongrain, A. Duri, F. Sarrazin, Z. Cheng, G. Cristobal, M. Marquez, D.A. Weitz, Electric control of droplets in microfluidic devices, Angew. Chem. Int. Ed. 45 (16) (2006) 2556–2560.
[11] R. Allan, S. Mason, Particle behaviour in shear and electric fields i. deformation and burst of fluid drops, Proceedings of the Royal Society of London. Series A. Mathematical and Physical Sciences 267 (1328) (1962) 45–61.
[12] C. Garton, Z. Krasucki, Bubbles in insulating liquids: stability in an electric field, Proceedings of the Royal Society of London. Series A. Mathematical and Physical Sciences 280 (1381) (1964) 211–226.
[13] G.I. Taylor, Studies in electrohydrodynamics. i. the circulation produced in a drop by an electric field, Proceedings of the Royal Society of London. Series A. Mathematical and Physical Sciences 291 (1425) (1966) 159–166.
[14] E. Lac, G. Homsy, Axisymmetric deformation and stability of a viscous drop in a steady electric field, J. Fluid Mech. 590 (2007) 239.
[15] O. Ajayi, A note on taylor's electrohydrodynamic theory, Proceedings of the Royal Society of London. A. Mathematical and Physical Sciences 364 (1719) (1978) 499–507.
[16] J. Sherwood, Breakup of fluid droplets in electric and magnetic fields, J. Fluid Mech. 188 (1988) 133–146.
[17] N. Dubash, A. Mestel, Behaviour of a conducting drop in a highly viscous fluid subject to an electric field, J. Fluid Mech. 581 (2007) 469.
[18] J.A. Lanauze, L.M. Walker, A.S. Khair, The influence of inertia and charge relaxation on electrohydrodynamic drop deformation, Phys. Fluids 25 (11) (2013) 112101.
[19] J.A. Lanauze, L.M. Walker, A.S. Khair, Nonlinear electrohydrodynamics of slightly deformed oblate drops, J. Fluid Mech. 774 (2015) 245–266.
[20] N. Dubash, A.J. Mestel, Breakup behavior of a conducting drop suspended in a viscous fluid subject to an electric field, Phys. Fluids 19 (7) (2007) 072101.
[21] R. Karyappa, S. Deshmukh, R. Thaokar, Breakup of a conducting drop in a uniform electric field, Journal of fluid mechanics 754 (2014) 550.
[22] O. Vizika, D. Saville, The electrohydrodynamic deformation of drops suspended in liquids in steady and oscillatory electric fields, Journal of fluid Mechanics 239 (1992) 1–21.
[23] J.-W. Ha, S.-M. Yang, Effects of surfactant on the deformation and stability of a drop in a viscous fluid in an electric field, Journal of colloid and interface science 175 (2) (1995) 369–385.
[24] J.-W. Ha, S.-M. Yang, Effect of nonionic surfactant on the deformation and breakup of a drop in an electric field, Journal of colloid and interface science 206 (1) (1998) 195–204.
[25] K.E. Teigen, S.T. Munkejord, Influence of surfactant on drop deformation in an electric field, Phys. Fluids 22 (11) (2010) 112104.
[26] H. Nganguia, Y.-N. Young, P.M. Vlahovska, J. Blawzdziewicz, J. Zhang, H. Lin, Equilibrium electro-deformation of a surfactant-laden viscous drop, Phys. Fluids 25 (9) (2013) 092106.
[27] H. Nganguia, O.S. Pak, Y.-N. Young, Effects of surfactant transport on electrodeformation of a viscous drop, Phys. Rev. E 99 (6) (2019) 063104.
[28] C. Sorgentone, A.-K. Tornberg, P.M. Vlahovska, A 3d boundary integral method for the electrohydrodynamics of surfactant-covered drops, J. Comput. Phys. 389 (2019) 111–127.
[29] L. Scriven, Dynamics of a fluid interface equation of motion for newtonian surface fluids, Chem. Eng. Sci. 12 (2) (1960) 98–108.
[30] J.P. Rane, V. Pauchard, A. Couzis, S. Banerjee, Interfacial rheology of asphaltenes at oil–water interfaces and interpretation of the equation of state, Langmuir 29 (15) (2013) 4750–4759.
[31] J.D. Jackson, Classical electrodynamics john wiley & sons, Inc., New York 13 (1999).
[32] L. Goual, A. Firoozabadi, Measuring asphaltenes and resins, and dipole moment in petroleum fluids, AIChE J. 48 (11) (2002) 2646–2663.
[33] H. Groenzin, O.C. Mullins, Molecular size and structure of asphaltenes from various sources, Energy & Fuels 14 (3) (2000) 677–684.
[34] K.J. Miller, J. Savchik, A new empirical method to calculate average molecular polarizabilities, J. Am. Chem. Soc. 101 (24) (1979) 7206–7213.
[35] D. Harbottle, Q. Chen, K. Moorthy, L. Wang, S. Xu, Q. Liu, J. Sjoblom, Z. Xu, Problematic stabilizing films in petroleum emulsions: Shear rheological response of viscoelastic asphaltene films and the effect on drop coalescence, Langmuir 30 (23) (2014) 6730–6738.
[36] C. Pozrikidis, A practical guide to boundary element methods with the software library BEMLIB, CRC Press, 2002.
[37] J. Rallison, A. Acrivos, A numerical study of the deformation and burst of a viscous drop in an extensional flow, J. Fluid Mech. 89 (1) (1978) 191–200.
[38] C. Pozrikidis et al., Boundary integral and singularity methods for linearized viscous flow, Cambridge University Press, 1992.
[39] M. Abramowitz, I.A. Stegun, Handbook of mathematical functions, Dover Publications, New York, 1965, p. 920.
[40] H.A. Stone, L.G. Leal, Relaxation and breakup of an initially extended drop in an otherwise quiescent fluid, J. Fluid Mech. 198 (1989) 399–427.
[41] D. Barthes-Biesel, A. Acrivos, Deformation and burst of a liquid droplet freely suspended in a linear shear field, J. Fluid Mech. 61 (1) (1973) 1–22.
[42] X. Li, D. Barthes-Biesel, A. Helmy, Large deformations and burst of a capsule freely suspended in an elongational flow, Journal of fluid mechanics 187 (1988) 179–196.
[43] E. Lac, D. Barthes-Biesel, N. Pelekasis, J. Tsamopoulos, Spherical capsules in three-dimensional unbounded stokes flows: effect of the membrane constitutive law and onset of buckling, J. Fluid Mech. 516 (2004) 303.
[44] D. Wasan, H. Brenner, D. Edward, Interfacial transport processes and rheology, Butterworth-Heinemann Series, Chem. Eng. (1991).
[45] J.B. Fenn, M. Mann, C.K. Meng, S.F. Wong, C.M. Whitehouse, Electrospray ionization for mass spectrometry of large biomolecules, Science 246 (4926) (1989) 64–71.
[46] R. Aris, Vectors, tensors and the basic equations of fluid mechanics, Courier Corporation (2012).